

How does “Which Way” Detector affect Fano Effect in Mesoscopic Transport —“Phonon-Fano” Or Not

Hai-Zhou Lu,^{1,*} Zuo-zi Chen,¹ Rong Lü,¹ and Bang-fen Zhu^{1,2,†}

¹*Center for Advanced Study, Tsinghua University, Beijing 100084, China*

²*Department of Physics, Tsinghua University, Beijing 100084, China*

(Dated: July 15, 2021)

We investigate the Fano interference in the presence of a “which way” detector, i.e., a local electron-phonon coupler, in the context of mesoscopic transport. Special attention is paid to study whether the phonon sidebands in the differential conductance spectra exhibit the typical lineshape of the Fano interference. When using a double-dot model we obtain two seemly contradictory results by slightly different approaches: The Markovian approach leads to *absolutely no* Fano interference at the phonon sidebands, while the Non-Markovian approach results in *finite* Fano interference at the phonon sidebands. On the other hand, by using the usual Aharonov-Bohm (AB)-ring model, i.e., only one dot is embedded into one arm of an AB-ring, only the Non-Markovian results are recovered. We explain these contradictory results and make a comparison between the double-dot model and the usual AB-ring model at length. Moreover, we also point out the essential difference between the manifestation of the “which way” effect in mesoscopic double-slit experiments and its optical counterpart.

PACS numbers: 73.63.-b, 73.21.La, 85.65.+h, 71.38.-k

I. INTRODUCTION

Thanks to rapid advances in nanotechnology, quantum coherence can be well maintained while electrons transport through a variety of mesoscopic systems.¹ Many coherent effects can thus be observed and investigated in mesoscopic systems. For instance, in a double-slit setup realized by using an Aharonov-Bohm (AB) ring with a quantum dot (QD) embedded,^{2,3} the interference between the resonant channel (the QD) and the continuum channel (the reference arm) will result in a typical asymmetric Fano resonance in the differential conductance spectra,⁴ because the phase of an electron would change by π when crossing a resonant level, compared with little phase shift in the continuum channel.

As a vivid illustration of the Bohr’s complementarity principle in quantum mechanics, in an optical Young’s double-slit experiment as shown in Fig. 1(a) if one detects which slit the photon passes through (even in principle), the interference pattern on the manifest screen will be destroyed. Candidates to realize such “which way” detector in mesoscopic systems in principle can be a diversity of scattering mechanisms, such as the electron-electron interaction induced spin flip⁵ and Coulomb repulsion,⁶ the light radiation,⁷ the electron-phonon interaction (EPI),^{8,9,10} etc. Since these mechanisms play important roles in transport in mesoscopic systems, to study how the “which way” detector affects the interference (e.g. Fano effect) would be crucial to understand the fundamental decoherence process in mesoscopic systems and would shed light on the potential applications.

To address this subject, we introduce a double-dot interferometer^{11,12} as depicted in Fig. 1(b). Specifically, the QD here is assumed to be a single-molecule coupled to two metallic electrodes. The phonon sidebands in the differential conductance are introduced by strong coupling between the electron and local optical vibration mode within the single-molecule.^{9,13,14,15,16,17,18,19} This model is ideal to deal with the “which way” problem: The theoretical deriva-

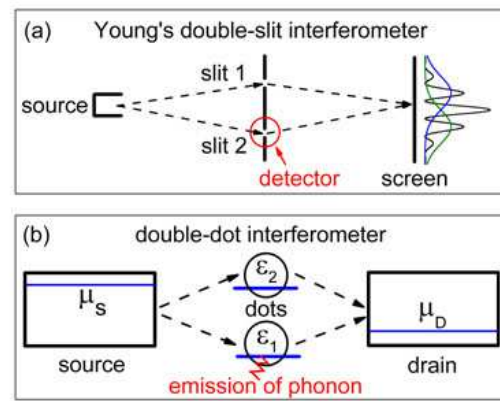


FIG. 1: (Color online)(a) Illustration of the “which way” effect in the Young’s double-slit experiment. (b) Configuration of the double-dot interferometer, where only dot 1 is coupled to a local optical phonon mode.

tion is much simplified compared to the usual one-dot AB-ring setup adopted in most works^{20,21} yet captures the essential physics. For general purpose, in the end we will compare this double-dot model with the usual AB-ring model in which only one QD is embedded in the AB-ring arms. We will see that, with minor modifications, our results can apply equally well to other interference models with the setup changed or the “which way” detector replaced.

As far as we know, most of previous publications mainly discuss how the “which way” detector affects the interference between elastic channels (the zero-phonon channel in our case), such as the visibility of AB oscillation¹² or the lineshape of the Fano resonance,²¹ etc; few attentions have been paid to the coherence of inelastic channels (phonon-assisted channels here).^{20,21,22} Regarding this, in this article we intend to investigate the coherence through the inelastic channels by examining whether the Fano interference survives in the dif-

ferential conductance spectra after a phonon is emitted (absorbed). The concern over the Fano lineshape in phonon sidebands has already been studied in Raman spectra of doped semiconductors.^{23,24} We shall show that by two slightly different approaches two incompatible results are obtained in the conductance spectra of the double-dot model. By the first approach that deals with the Markovian case, the phonon sidebands give *absolutely no* hint of the Fano interference; while by the second approach that suits to the Non-Markovian case, the phonon sidebands do exhibit Fano interference to certain extent. On the other hand, for the one-dot AB-ring setup, only the Non-Markovian results can be recovered.^{20,21} Compared to the usual Young's double-slit experiment, it seems that the Markovian result agrees with the "which way" rule, while the Non-Markovian result violates it. By carefully examining the electron-phonon decoupling process, we have found the key to these incompatible results. We will show that the usual AB-ring model only works for one circumstance while the double-dot model can capture both. We will also point out that the coherent multi-reflection would be responsible for the different manifestations of "which way" effect in mesoscopic double-slit interferometer and its optical analogy.

II. MODEL

The Hamiltonian for the double-dot interferometer depicted in Fig. 1(b) can be expressed as

$$\mathbf{H} = \sum_{\mathbf{k}, \eta \in S, D} \varepsilon_{\eta \mathbf{k}} \mathbf{c}_{\eta \mathbf{k}}^\dagger \mathbf{c}_{\eta \mathbf{k}} + \sum_{i \in 1, 2} \varepsilon_i \mathbf{d}_i^\dagger \mathbf{d}_i + \lambda \mathbf{d}_1^\dagger \mathbf{d}_1 (\mathbf{a}^\dagger + \mathbf{a}) + \hbar \omega_0 \mathbf{a}^\dagger \mathbf{a} + \sum_{\eta \mathbf{k} i} (V_{\eta \mathbf{k} i} \mathbf{c}_{\eta \mathbf{k}}^\dagger \mathbf{d}_i + h.c.). \quad (1)$$

Here $\mathbf{c}_{\eta \mathbf{k}}^\dagger$ ($\mathbf{c}_{\eta \mathbf{k}}$) is the creation (annihilation) operator for an electron with wave vector \mathbf{k} in the lead η [$\eta = S(D)$ stands for the source (drain) lead], and \mathbf{d}_i^\dagger (\mathbf{d}_i) is the creation (annihilation) operator of an electron residing in the dot i . The spin index is omitted here for simplicity. Phonon operator \mathbf{a}^\dagger (\mathbf{a}) creates (annihilates) a local optical vibration in dot 1 at frequency ω_0 with the EPI strength λ . Electron can tunnel between the lead η and dot i with a hopping amplitude denoted as $V_{\eta \mathbf{k} i}$. By denoting the chemical potential in each lead as μ_η , we express the gate voltage as $V_{\text{mid}} = (\mu_S + \mu_D)/2e$, and the bias voltage as $V_{\text{bias}} = (\mu_S - \mu_D)/e$.

Within the nonequilibrium Green function formalism the steady current tunneling through the interferometer can be expressed as,²⁵

$$J = J^{\text{sum}} + J^{\text{inte}}, \quad (2)$$

where

$$J^\delta \equiv (J_S^\delta - J_D^\delta)/2, \quad (3)$$

with $\delta = \text{sum, inte}$. For later convenience of studying the interference phenomena, we separate the total current J into two parts: the sum of currents through two channels J^{sum} , and the

interference between two channels J^{inte} , i.e.,

$$J_\eta^{\text{sum}} = \frac{e}{h} \int d\omega \sum_i \Gamma_{ii}^\eta(\omega) \{f_\eta(\omega) A_{ii}(\omega) + iG_{ii}^<(\omega)\}, \quad (4)$$

$$J_\eta^{\text{inte}} = \frac{e}{h} \int d\omega \sum_i \Gamma_{\bar{i}i}^\eta(\omega) [f_\eta(\omega) A_{\bar{i}i}(\omega) + iG_{\bar{i}i}^<(\omega)], \quad (5)$$

where $G_{ij}^{r(a)}$ and $G_{ij}^{>(<)}$ are respectively the retarded (advanced) and the greater (lesser) Green functions of the dot region, the index $\bar{i} = 2(1)$ if $i = 1(2)$, $A_{ij}(\omega)$ is the spectral function defined via $A_{ij} = i(G_{ij}^> - G_{ij}^<)$, and $\Gamma_{ij}^\eta(\omega)$ is the broadening function defined as $2\pi \sum_{\mathbf{k}} V_{\eta \mathbf{k} i}^* V_{\eta \mathbf{k} j} \delta(\varepsilon_{\eta \mathbf{k}} - \omega)$. In the following, we shall derive these Green functions by using the equation of motion method and disentangle the electron-phonon part via the canonical transformation. The differential conductance, $\mathbf{G} \equiv \mathbf{G}^{\text{sum}} + \mathbf{G}^{\text{inte}}$, can be obtained accordingly via

$$\mathbf{G}^{\text{sum}} = \partial_{V_{\text{bias}}} J^{\text{sum}}, \quad \mathbf{G}^{\text{inte}} = \partial_{V_{\text{bias}}} J^{\text{inte}}. \quad (6)$$

We shall show that each peak in the summation term \mathbf{G}^{sum} corresponds to a channel that electron tunnels through, and the hump and dip structure at corresponding energy in the interference term \mathbf{G}^{inte} can be used to identify whether two channels interfere with each other or not.

III. FANO EFFECT WITHOUT EPI ($\lambda = 0$)

In the absence of EPI, we can reduce the Hamiltonian in Eq. (1) to the Fano-Anderson Hamiltonian, whereby we obtain the retarded Green's functions rigorously by the equation of motion approach,

$$G_{ij}^{0,r}(\omega) = \frac{1}{Q} \begin{pmatrix} \omega - \varepsilon_2 + i\Gamma_{22}/2, & -i\Gamma_{12}/2 \\ -i\Gamma_{21}/2, & \omega - \varepsilon_1 + i\Gamma_{11}/2 \end{pmatrix}, \quad (7)$$

where

$$\Gamma_{ij} \equiv \Gamma_{ij}^S + \Gamma_{ij}^D,$$

and

$$Q \equiv (\omega - \varepsilon_1 + i\Gamma_{11}/2)(\omega - \varepsilon_2 + i\Gamma_{22}/2) + \Gamma_{12}\Gamma_{21}/4.$$

The superscript zero of the Green's function here denotes the absence of EPI ($\lambda = 0$). We then obtain the spectral function $A_{ij}^0(\omega) = -2\Im\{G_{ij}^{0,r}(\omega)\}$, the advanced Green's functions $G_{ji}^{0,a}(\omega) = (G_{ij}^{0,r}(\omega))^*$, and the greater (lesser) Green's functions via the Keldysh formula as $G_{ij}^{0,>(<)}/(\omega) = \sum_{mn} G_{im}^{0,r}(\omega) \Sigma_{mn}^{0,>(<)}/(\omega) G_{nj}^{0,a}(\omega)$, where $\Sigma_{ij}^{0,<}(\omega) = i \sum_\eta f_\eta(\omega) \Gamma_{ij}^\eta$, and $\Sigma_{ij}^{0,>} = \Sigma_{ij}^{0,<} - i\Gamma_{ij}$. By substituting the expressions above into Eqs.(3)-(6) we obtain the required currents and conductances.

The zero-temperature differential conductance through the double dots without EPI is plotted in Fig. 2 as a function of the bias voltage V_{bias} and gate voltage V_{mid} . The typical asymmetric lineshape in the differential conductance is the

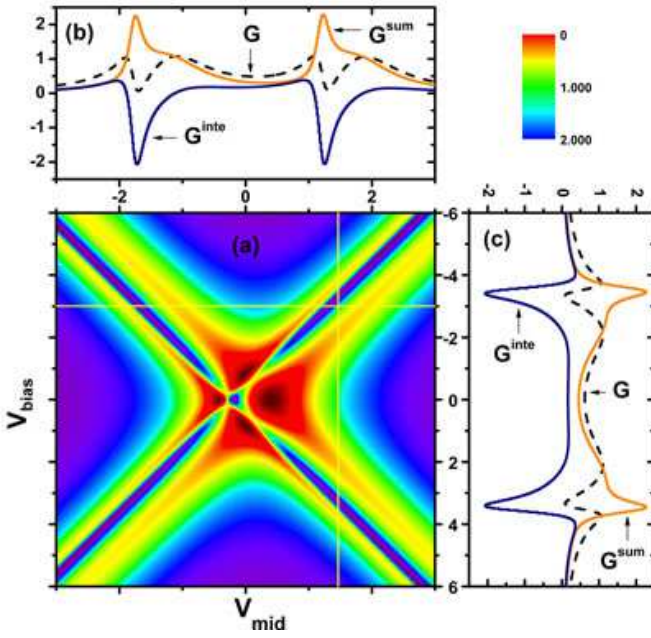


FIG. 2: (Color online)(a) The zero-temperature differential conductance \mathbf{G} as a function of V_{bias} and V_{mid} in the absence of EPI. (b) and (c) are section profiles for fixed V_{bias} and V_{mid} , respectively. Here the interference component \mathbf{G}^{inte} (black solid lines) of the total conductance \mathbf{G} (dashed lines) as well as the sum of the conductance through dot 1 and 2 (\mathbf{G}^{sum} , yellow solid lines) are plotted in the same panels for comparison. Throughout the paper the phonon frequency $\hbar\omega_0$ is set as the energy unit. Other parameters used are $\varepsilon_1 = -0.4$, $\varepsilon_2 = 0.4$, $\Gamma_{11} = 0.2$, $\Gamma_{22} = 0.6$, $\Gamma_{12} = \Gamma_{21} = \sqrt{\Gamma_{11}\Gamma_{22}}$.

manifestation of the Fano interference between two channels through the double dots, which has already been extensively discussed in the previous publication.^{11,26,27} The interference pattern will switch from the constructive to the destructive whenever the incident electron experiences a π phase change in channel 1 (through crossing the resonance level ε_1 in dot 1) while remains its phase in the reference channel (dot 2). We also plot the corresponding \mathbf{G}^{sum} and \mathbf{G}^{inte} in the section profiles for comparison. As clearly shown by the curves, every time \mathbf{G} exhibits the asymmetric Fano lineshape, the interference term \mathbf{G}^{inte} will exhibit the hump and dip structure, which can also be viewed as an evidence of the Fano interference.

IV. FANO EFFECT WITH EPI ($\lambda \neq 0$)

In order to treat the EPI unperturbatively, we employ the standard canonical transformation technique²⁸ to eliminate the electron-phonon coupling terms in the Hamiltonian Eq. (1). Namely, let $\mathbf{S} \equiv \lambda \mathbf{d}_1^\dagger \mathbf{d}_1 (\mathbf{a}^\dagger - \mathbf{a}) / \hbar\omega_0$, the transformed Hamiltonian reads

$$\tilde{\mathbf{H}} = e^{\mathbf{S}} \mathbf{H} e^{-\mathbf{S}} \equiv \tilde{\mathbf{H}}_{\text{ph}} + \tilde{\mathbf{H}}_{\text{el}}.$$

In the transformation, the phonon part keeps unchanged, while the electron part is reshaped into

$$\tilde{\mathbf{H}}_{\text{el}} = \sum_{\eta\mathbf{k}} \varepsilon_{\eta\mathbf{k}} \mathbf{c}_{\eta\mathbf{k}}^\dagger \mathbf{c}_{\eta\mathbf{k}} + \sum_i \bar{\varepsilon}_i \mathbf{d}_i^\dagger \mathbf{d}_i + \sum_{\eta\mathbf{k}i} (\bar{V}_{\mathbf{k}i}^\eta \mathbf{c}_{\eta\mathbf{k}}^\dagger \mathbf{d}_i + h.c.), \quad (8)$$

where $\bar{\varepsilon}_2 = \varepsilon_2$, $\bar{\varepsilon}_1 \equiv \varepsilon_1 - \lambda^2 / \hbar\omega_0$, $\bar{V}_{\mathbf{k}2}^\eta = V_{\mathbf{k}2}^\eta$, and $\bar{V}_{\mathbf{k}1}^\eta \equiv V_{\mathbf{k}1}^\eta \mathbf{X} \equiv V_{\mathbf{k}1}^\eta \exp(-\lambda(\mathbf{a}^\dagger - \mathbf{a}) / \hbar\omega_0)$. It is noticed that the transformed hopping amplitude contains the phonon operator \mathbf{X} , indicating that the electron and phonon are still entangled during hopping processes. The usual practice as a first-order approximation is replacing the phonon operator with its mean-field expectation value, i.e.,

$$\bar{V}_{\mathbf{k}\eta,1} \approx V_{\mathbf{k}\eta,1} \langle \mathbf{X} \rangle = V_{\mathbf{k}\eta,1} e^{-\phi_0}, \quad (9)$$

where $\phi_0 \equiv g(N_{\text{ph}} + 1/2)$, $g \equiv (\lambda/\omega_0)^2$ and N_{ph} denotes the phonon occupation which obeys the Bose distribution at temperature T . By this polaron approximation, electrons are decoupled from phonons, and $\tilde{\mathbf{H}}_{\text{el}}$ is transformed into the Fano-Anderson Hamiltonian with the parameters renormalized. Hereafter we denote the Green's functions defined in the context of $\tilde{\mathbf{H}}_{\text{el}}$ by adding a small bar overhead, i.e., \bar{G}_{ij} , which can be readily expressed with G_{ij}^0 in Eq. (7) by replacing the superscript zero with a small bar.

In the following, we shall discuss two slightly different approaches to evaluate the full Green functions $G_{ij}^{r(a,>,<)}$ from the $\bar{G}_{ij}^{r(a,>,<)}$.

The first one is straightforward.²⁹ By using Eq. (9) and the relation like $\langle \mathbf{d}_i(t) \mathbf{d}_j^\dagger(t') \rangle = \langle \bar{\mathbf{d}}_i(t) \bar{\mathbf{d}}_j^\dagger(t') \rangle \langle \mathbf{X}(t) \mathbf{X}^\dagger(t') \rangle$, we decouple the Green functions³⁰ and obtain the intra-dot Green functions as

$$\begin{aligned} G_{11}^{>(<)}(\omega) &= \sum_n L_n \bar{G}_{11}^{>(<)}(\omega \mp n\omega_0), \\ G_{22}^{>(<)}(\omega) &= \bar{G}_{22}^{>(<)}(\omega). \end{aligned} \quad (10)$$

Here

$$L_n \equiv e^{n\omega_0\beta/2} e^{-(g(2N_{\text{ph}}+1))} I_n \left[2g \sqrt{N_{\text{ph}}(N_{\text{ph}}+1)} \right],$$

in which $I_n(z)$ is the n -th Bessel function of complex argument z , and $\beta = 1/k_B T$. Since only the electron in dot 1 is subjected to the EPI, $\langle \mathbf{d}_1(t) \mathbf{d}_2^\dagger(t') \rangle = \langle \bar{\mathbf{d}}_1(t) \bar{\mathbf{d}}_2^\dagger(t') \rangle \langle \mathbf{X}(t) \mathbf{X}^\dagger(t') \rangle$, and the inter-dot Green functions then read

$$G_{12}^{>(<)} = \bar{G}_{12}^{>(<)} e^{-\phi_0}, \quad G_{21}^{>(<)} = \bar{G}_{21}^{>(<)} e^{-\phi_0}. \quad (11)$$

The differential conductances with finite EPI obtained by the first approach are plotted in Fig. 3. Compared with the non-EPI case, both \mathbf{G} and \mathbf{G}^{sum} demonstrate a set of sidebands at $\bar{\varepsilon}_1 \pm n\hbar\omega_0$, which are mathematically related with the phonon expansions in $G_{11}^{>(<)}$ and come from the phonon correlation functions $\langle \mathbf{X}(t) \mathbf{X}^\dagger(t') \rangle_{\text{ph}}$ or the $\langle \mathbf{X}^\dagger(t') \mathbf{X}(t) \rangle_{\text{ph}}$. However, the inter-dot correlation functions obtained in this way only contain $\langle \mathbf{X}(t) \rangle_{\text{ph}}$ or $\langle \mathbf{X}^\dagger(t') \rangle_{\text{ph}}$, thus $G_{ii}^{>(<)}$ can not be expanded into similar phonon series. As a result, besides the hump and

dip near $\bar{\varepsilon}_1$, \mathbf{G}^{inte} exhibits no side-peak structure at $\bar{\varepsilon}_1 \pm n\hbar\omega_0$, and \mathbf{G} shows no Fano interference feature at the phonon sidebands either. This means that the phonon channel through dot 1 does not interfere with the reference channel through dot 2, unlike the zero-phonon channel.

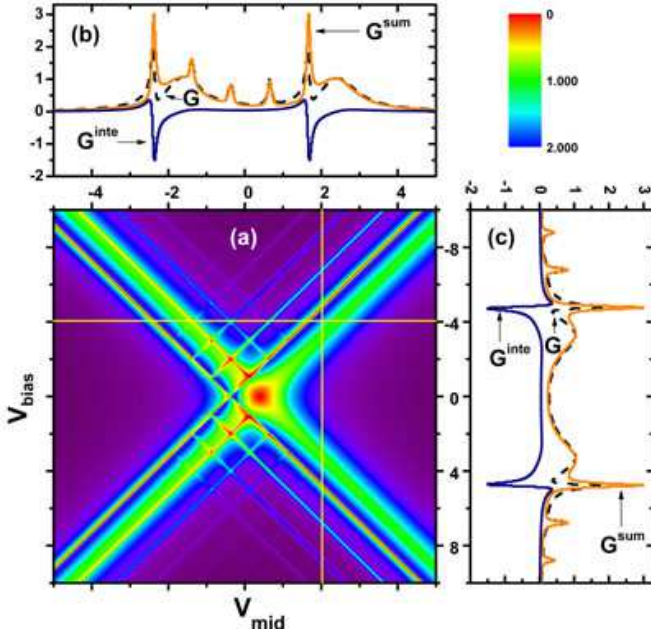


FIG. 3: (Color online) The differential conductance obtained by the Markovian approach in the presence of EPI ($\lambda = 1$), with the parameters and line notation same with Fig. 2.

If we assume that no phonon is involved in the tunneling process of electron through dot 2, the result above seems reasonable and agrees with the “which way” rule. In this case, phonon-assisted channel is in principle recognized if the emitted or absorbed phonon is detected. As a result the phonon-assisted channel will not interfere with the elastic reference channel, and G shows no interfere feature at phonon side-peaks. However, these statements are true only under the assumption that the electron is *not* coupled to phonons *at all* when passing the reference channel, as in the case of Young’s two-slit interfere experiment. To justify whether the assumption is valid, we need to clarify two different situations in usual mesoscopic systems, which critically depends on the coherent properties of the leads: (i) The Markovian leads, into which the electrons will lose their phase memory completely, namely the electrons which originally come from dot 1 forget their previous coupling with phonons once entering into both leads and dot 2; (ii) The Non-Markovian leads, into which the electron still keep its phase memory to some extent, namely the electron in dot 2 will be coupled to phonons as the electron in dot 1 through a coherent multi-reflection process. Clearly the first approach is the Markovian approach, which suits for the cases with the Markovian leads and certainly not for the Non-Markovian leads.

To account for the Non-Markovian lead, we modify the first approach a little bit. More specific, we will modify the

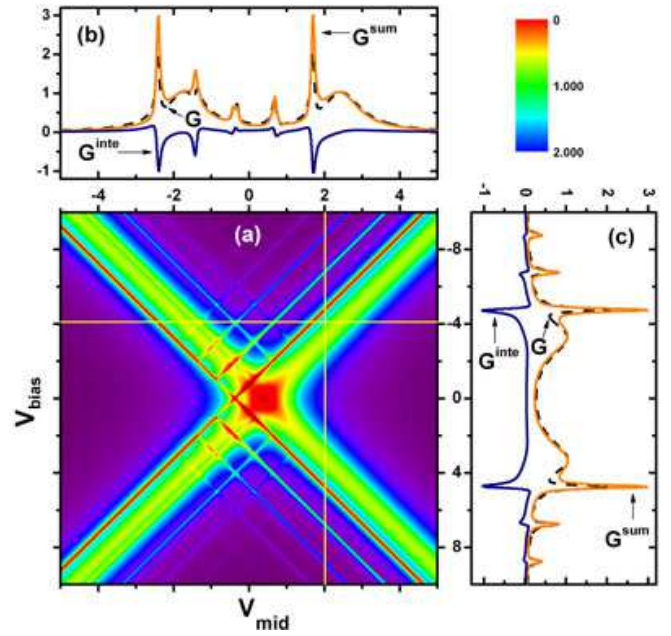


FIG. 4: (Color online) The differential conductance obtained by the Non-Markovian approach in the presence of EPI ($\lambda = 1$), with the same parameters and line notation as in Fig. 3.

way of decoupling the electrons from phonons. The previous usage of Eq. (9) decouples the lead electrons from phonons completely, thus no entanglement between the electron in dot 2 and phonons needs considering in subsequent derivations. To avoid this for the Non-Markovian case, we shall derive the inter-dot correlation function before taking the electron-phonon decoupling approximation. In the following, we shall outline our derivation for the Non-Markovian case, but leave the details in the Appendix.

Firstly, with the help of the equation of motion we can express the inter-dot correlation functions $G_{ij}^{>(<)}$ in terms of the intra-dot Green function $G_{ii}^{>(<)}$ as

$$\begin{aligned} G_{12}^{>(<)}(\omega) &= G_{11}^{>(<)}\omega s_{12}^a(\omega) + G_{11}^r(\omega)p^{>(<)}\omega, \\ G_{21}^{>(<)}\omega &= s_{21}^r(\omega)G_{11}^{>(<)}\omega + q^{>(<)}\omega G_{11}^a(\omega), \end{aligned} \quad (12)$$

where the functions $s_{ij}^{r(a)}$ and $q(p)^{>(<)}$ can be found in the Appendix A. Secondly, by using the same electron-phonon decoupling approximation [Eq. (9)] and similar procedure as in the Markovian approach, we get the intra-dot Green functions $G_{ii}^{>(<)}$ as in Eq. (10) and $G_{11}^{r(a)}$ via

$$G_{ii}^{r(a)}(\omega) = P \int_{-\infty}^{\infty} \frac{d\omega'}{2\pi} \frac{A_{ii}(\omega)}{\omega - \omega'} \mp \frac{i}{2} A_{ii}(\omega). \quad (13)$$

Finally, we substitute $G_{11}^{r(a),>(<)}$ back into Eq. (12) and obtain all the required Green functions. It is noticed that by this modified decoupling procedure, the inter-dot correlation functions also contain the terms of $\langle \mathbf{X}^\dagger(t)\mathbf{X}(t') \rangle_{\text{ph}}$ and can be expanded into phonon series. Therefore the entanglement between phonons and electrons in dot 2 are partially maintained via coherent multi-reflection.

Differential conductance calculated with the Non-Markovian approach is plotted in Fig. 4. Compared with the Markovian results in Fig. 3, we have found \mathbf{G}^{sum} remains unchanged, while \mathbf{G}^{int} contains some phonon structures that are totally absent in Fig. 3. This indicates that the phonon-assisted tunneling channel through dot 1 does interfere with the reference channel through dot 2, so certain Fano lineshape appears in the phonon side-peaks of the differential conductance \mathbf{G} , as obtained in previous results in the AB-ring setup.^{20,21}

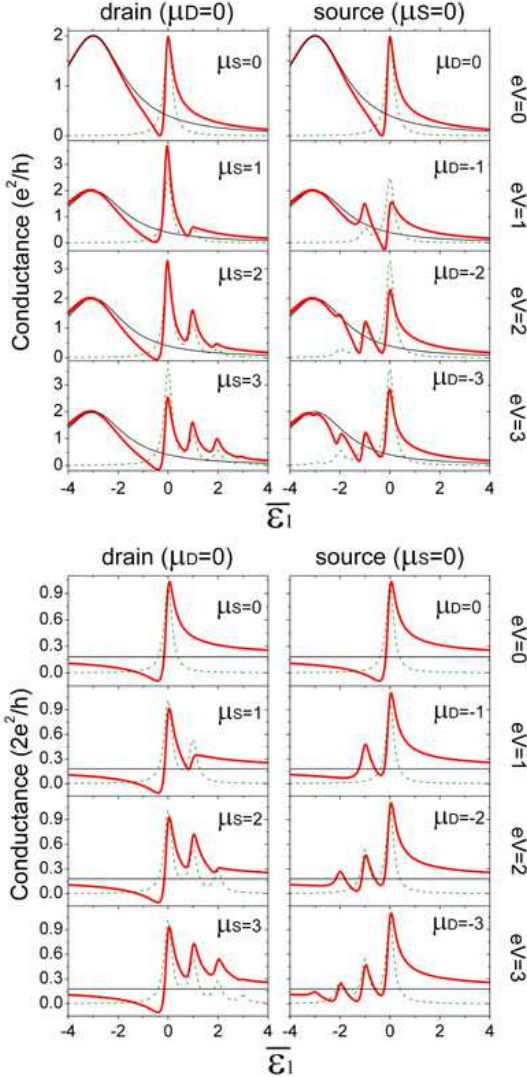


FIG. 5: (Color online) Comparison between results of the double-dot interferometer by the non-Markovian approach (upper 8 panels) and the AB-ring model (lower 8 panels). The conductances contributed from the source and drain leads are plotted in the left and right panels, respectively, in which the thick solid lines represent the total conductance, the thin dash lines stand for the conductance when only the dot 1 channel is open, and the thin solid lines are the conductance when only the dot 2 in the double-dot system or the reference channel in the AB-ring model is conducting. The parameters for the double-dot are $3\Gamma_{11}^{\text{S/D}} = \Gamma_{22}^{\text{S/D}} = 0.5$, $\epsilon_2 = \bar{\epsilon}_1 + 3$, and that for the AB-ring are $\Gamma_S = \Gamma_D = 0.5$, $\xi = 0.05$, $\phi = 0$.

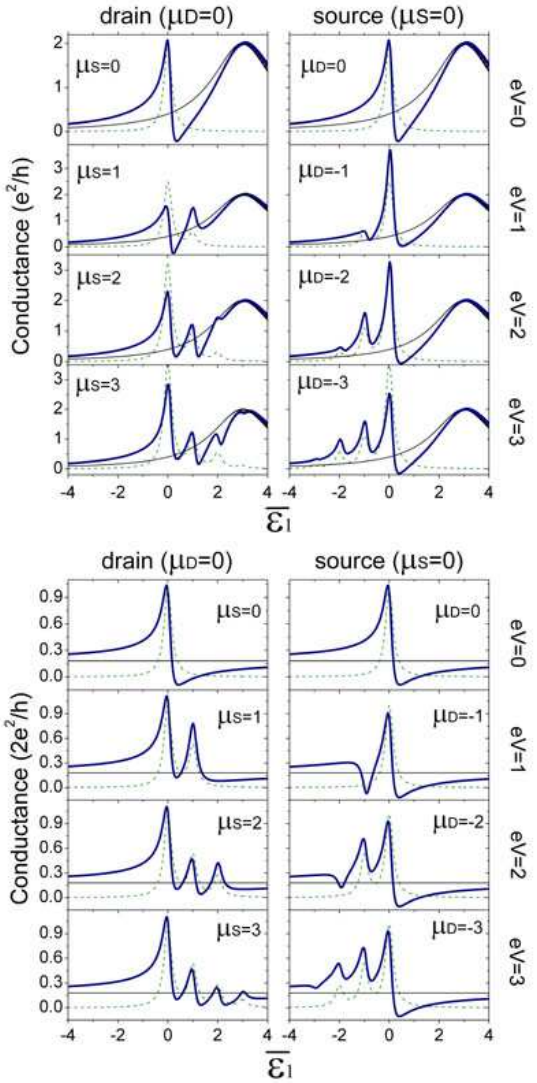


FIG. 6: (Color online) The same as in Fig. 5 except $\phi = \pi$ for the AB-ring model and $\epsilon_2 = \bar{\epsilon}_1 - 3$ for the double-dot model.

V. COMPARISON BETWEEN AB-RING AND DOUBLE-DOT WITH NON-MARKOVIAN APPROACH

Above results are generally true for other multi-channel interfere systems with local “which way” detector. For example, we calculate the differential conductance in a usual AB-ring model as given in Appendix B, and compare the results with the double-dot interference system calculated with the Non-Markovian approach (Figs. 5 and 6). For better comparison to the previous work,²¹ we plot the differential conductance spectra as functions of $(\bar{\epsilon}_1 - \mu_{S/D})$ at several fixed bias voltage $eV = \mu_S - \mu_D$, which is increased from the top to the bottom in the figures. It is worth pointing out that here we have used the improved electron-phonon decoupling scheme for the Green functions,³⁰ so we can deal with the bias-induced phonon-assisted processes at low temperature more appropriately. As a consequence, the differential con-

ductance at zero temperature exhibit phonon sidepeaks at both sides of the zero-phonon peaks, which is quite different from the previous work.²¹ To clearly show the improvements, we measure the conductance by the source and drain Fermi levels on the left and right columns, respectively. Technically, they are obtained by $\lim_{\delta \rightarrow 0} [I(\bar{\varepsilon}_1, \mu_D) - I(\bar{\varepsilon}_1, \mu_D - \delta)]/\delta$ and $\lim_{\delta \rightarrow 0} [I(\bar{\varepsilon}_1, \mu_S + \delta) - I(\bar{\varepsilon}_1, \mu_S)]/\delta$.

As shown in Figs. 5 and 6, in the AB-ring model the Fano-asymmetric lineshapes also appear in the phonon sidepeaks of the differential conductance, just like the Non-Markovian case for the double-dot model. The reason why the AB-ring model's result is similar to the Non-Markovian case rather than the Markovian case lies in its current formula Eq. (B5), which is obtained by integrating out the reference channels to get a formula in terms of the dot Green functions before taking any approximation to EPI. This procedure is essentially equivalent to the Non-Markovian approach we have adopted in the double-dot model, so it is no wonder why the AB-ring's result exhibits the similar Phonon-Fano lineshapes. Moreover, since the reference channel in the AB-ring model connects two leads directly, it is not easy to take into account the Markovian effect in the AB-ring model in contrasts to the double-dot model.

The main difference between two models is that the transmission probability through the reference channel is constant in the AB-ring model, while it varies as a function of energy in the double-dot model. Despite of this difference, one can easily identify the similarities between the results of $\varepsilon_2 = \bar{\varepsilon}_1 + 3$ (double-dot model) and $\phi = 0$ (AB-ring model) in Fig. 5, or $\varepsilon_2 = \bar{\varepsilon}_1 - 3$ (double-dot model) and $\phi = \pi$ (AB-ring model) in Fig. 6, because due to the Friedel's sum rule³¹ a π phase shift occurs for electron in dot 1 when its incident energy crosses $\bar{\varepsilon}_1$, which is equivalent to adding a π magnetic flux threading the AB-ring.

VI. CONCLUSION

In summary, the Fano effect in the presence of local electron-phonon coupling has been studied in a double quantum dot system compared to an AB-ring system. In contrast to its optical analogy, when tunneling into the leads in a mesoscopic systems, electrons can either lose their phase memory completely (Markov case) or maintain at least part of the coherence (Non-Markov case), which determines whether the coherent multi-reflection between different channels exists. As a consequence, the phonon sidebands in the differential conductance will not show the Fano interference for the Markov cases, or exhibit the Fano interference to certain extent for the Non-Markov cases. The double-dot model can describe both circumstances while the AB-ring model can only capture the Non-Markovian case. In the double-dot model, to account for both cases, the usual electron-phonon decoupling approximation should be treated with care.

Acknowledge: The authors would like to acknowledge Dr. Hui Zhai, Chao-Xing Liu, Prof. M. Eto and Dr. A. Ueda for helpful discussions. This research is supported by the NSFC (Grant 10574076), the Basic Research Program of

China (Grant No. 2006CB921500, 2006CB605105) and the MOE of China (Grant No.200221).

APPENDIX A: DERIVATION OF THE INTER-DOT CORRELATION FUNCTIONS

The inter-dot correlation functions can be derived as functions of the intra-dot Green functions by using the equations of motion method,

$$(-i\partial_{\tau'} - \varepsilon_2) G_{12}(\tau, \tau') = \sum_{\eta\mathbf{k}} V_{\eta\mathbf{k}2} G_{1,\eta\mathbf{k}}(\tau, \tau'). \quad (\text{A1})$$

The factor $(-i\partial_{\tau'} - \varepsilon_2)$ can be interpreted as the inverse operator of the noninteracting electron Green function of dot 2 multiplied from left, then we have

$$G_{12}(\tau, \tau') = \sum_{\eta\mathbf{k}} V_{\eta\mathbf{k}2} \int d\tau_1 G_{1,\eta\mathbf{k}}(\tau, \tau_1) g_2(\tau_1, \tau'). \quad (\text{A2})$$

Similarly,

$$G_{1,\eta\mathbf{k}}(\tau, \tau_1) = \sum_j V_{\eta\mathbf{k}j}^* \int d\tau_2 G_{1j}(\tau, \tau_2) g_{\eta\mathbf{k}}(\tau_2, \tau_1). \quad (\text{A3})$$

Combine these two equations, we have

$$G_{12}(\tau, \tau') = \sum_j \int d\tau_1 d\tau_2 G_{1j}(\tau, \tau_2) \Sigma_{j2}(\tau_2, \tau_1) g_2(\tau_1, \tau'),$$

where the self energy is defined as

$$\Sigma_{j2}(\tau_2, \tau_1) \equiv \sum_{\eta\mathbf{k}} V_{\eta\mathbf{k}j}^* g_{\eta\mathbf{k}}(\tau_2, \tau_1) V_{\eta\mathbf{k}2}. \quad (\text{A4})$$

To do analytic continuation for terms like $D = \int_C ABC$, we have the Langreth Theorem, i.e.,

$$\begin{aligned} D^> &= \int_t (A^r B^r C^> + A^r B^> C^a + A^> B^a C^a), \\ D^r &= \int_t A^r B^r C^r. \end{aligned} \quad (\text{A5})$$

Thus, after the analytic continuation and Fourier transformation, we have

$$\begin{aligned} G_{12}^<(\omega) &= \sum_j G_{1j}^r(\omega) [\Sigma_{j2}^r(\omega) g_2^<(\omega) + \Sigma_{j2}^<(\omega) g_2^a(\omega)] \\ &\quad + \sum_j G_{1j}^< \Sigma_{j2}^a(\omega) g_2^a(\omega), \\ G_{12}^r(\omega) &= \sum_j G_{1j}^r(\omega) \Sigma_{j2}^r(\omega) g_2^r(\omega). \end{aligned} \quad (\text{A6})$$

Further simplification shows that

$$G_{12}^<(\omega) = G_{11}^<(\omega) s_{12}^a(\omega) + G_{11}^r(\omega) p^<(\omega), \quad (\text{A7})$$

$$G_{12}^r(\omega) = G_{11}^r(\omega) s_{12}^r(\omega). \quad (\text{A8})$$

Similarly,

$$G_{21}^<(\omega) = s_{21}^r(\omega)G_{11}^<(\omega) + q^<(\omega)G_{11}^a(\omega), \quad (\text{A9})$$

$$G_{21}^a(\omega) = s_{21}^a(\omega)G_{11}^a(\omega). \quad (\text{A10})$$

After having the expressions for lesser Green functions, the greater Green functions can then be readily obtained just by replacing the $<$ to $>$ in the above expressions, i.e.,

$$G_{12}^>(\omega) = G_{11}^>(\omega)s_{12}^a(\omega) + G_{11}^r(\omega)p^>(\omega), \quad (\text{A11})$$

$$G_{21}^>(\omega) = s_{21}^r(\omega)G_{11}^a(\omega) + q^>(\omega)G_{11}^r(\omega). \quad (\text{A12})$$

Here the correlation functions $p^{>(<)}$, $q^{>(<)}$ and $s_{ij}^{r(a)}$ are defined as below,

$$\begin{aligned} p^{>(<)} &\equiv \frac{\Sigma_{12}^r g_2^{>(<)} + \Sigma_{12}^{>(<)} g_2^a}{(1 - \Sigma_{22}^r g_2^r)(1 - \Sigma_{22}^a g_2^a)} + \frac{\Sigma_{12}^r \Sigma_{22}^{>(<)} - \Sigma_{22}^r \Sigma_{12}^{>(<)}}{(1 - \Sigma_{22}^r g_2^r)(1 - \Sigma_{22}^a g_2^a)} g_2^r g_2^a, \\ q^{>(<)} &\equiv \frac{g_2^r \Sigma_{21}^< + g_2^{>(<)} \Sigma_{21}^a}{(1 - g_2^r \Sigma_{22}^r)(1 - g_2^a \Sigma_{22}^a)} + \frac{\Sigma_{21}^a \Sigma_{22}^{>(<)} - \Sigma_{22}^a \Sigma_{21}^{>(<)}}{(1 - g_2^r \Sigma_{22}^r)(1 - g_2^a \Sigma_{22}^a)} g_2^r g_2^a, \\ s_{ij}^{r(a)} &\equiv \frac{\Sigma_{ij}^{r(a)} g_2^{r(a)}}{1 - \Sigma_{22}^{r(a)} g_2^{r(a)}}. \end{aligned} \quad (\text{A13})$$

For cases where $V_{\eta\mathbf{k}i}$ is independent of \mathbf{k} , $\Sigma_{ij}^{r(a)} \Sigma_{22}^{>(<)} - \Sigma_{22}^{r(a)} \Sigma_{ij}^{>(<)}$ = 0 and the second term in the expressions of p or q vanishes.

APPENDIX B: MODEL AND DERIVATION OF AB-RING MODEL

The Hamiltonian of the AB-ring model reads^{21,32}

$$\mathbf{H}_{\text{AB}} = \mathbf{H}_{\text{leads}} + \mathbf{H}_{\text{D}} + \mathbf{H}_{\text{T}}, \quad (\text{B1})$$

where the lead part $\mathbf{H}_{\text{leads}}$ is the same as in the Eq. (1). The second term describes the single level coupled to the single vibrational mode

$$\mathbf{H}_{\text{D}} = \varepsilon_1 \mathbf{d}_1^\dagger \mathbf{d}_1 + \hbar \omega_0 \mathbf{a}^\dagger \mathbf{a} + \lambda \mathbf{d}_1^\dagger \mathbf{d}_1 (\mathbf{a}^\dagger + \mathbf{a}), \quad (\text{B2})$$

where the operators and parameters are of the same meaning as those in the double-dot interferometer. The last term

$$\mathbf{H}_{\text{T}} = \sum_{\mathbf{k}, \eta \in \text{S, D}} (V_{\eta\mathbf{k}1} \mathbf{c}_{\eta\mathbf{k}}^\dagger \mathbf{d}_1 + h.c.) + \sum_{\mathbf{k}, \mathbf{k}'} (W e^{i\phi} \mathbf{c}_{\mathbf{D}\mathbf{k}}^\dagger \mathbf{c}_{\mathbf{S}\mathbf{k}} + h.c.), \quad (\text{B3})$$

where the first part is the same as that in Eq. (1) while the second part depicts a direct tunneling between the source and drain leads. W is the lead-lead transmission amplitude assumed to be independent of momentum \mathbf{k} and \mathbf{k}' . ϕ is the flux threading the AB-ring, which can be assumed to be affiliated only to the lead-lead coupling due to the gauge invariance.

The current through an AB-ring with a dot embedded can be expressed as^{21,32}

$$I = \frac{2e}{h} \int d\omega [f_{\text{S}}(\omega) - f_{\text{D}}(\omega)] T(\omega), \quad (\text{B4})$$

where the transmission probability

$$\begin{aligned} T(\omega) &= \frac{4\xi}{(1 + \xi)^2} + \frac{2\text{Re}G_d^r(\omega)}{(1 + \xi)^3} [2(1 - \xi) \sqrt{\xi \Gamma_{\text{S}} \Gamma_{\text{D}}} \cos \phi] \\ &+ \frac{2\text{Im}G_d^r(\omega)}{\Gamma(1 + \xi)^3} [(\xi(\Gamma_{\text{S}}^2 + \Gamma_{\text{D}}^2) - \Gamma_{\text{S}} \Gamma_{\text{D}}(1 + \xi^2) + 4\xi \Gamma_{\text{S}} \Gamma_{\text{D}} \cos^2 \phi)]. \end{aligned}$$

Here $\Gamma_{\eta \in \{\text{S, D}\}} = 2\pi \sum_{\mathbf{k}} |V_{\eta\mathbf{k}1}|^2 \delta(\varepsilon_{\eta\mathbf{k}} - \omega)$ denotes the coupling between the dot and the source (drain) lead, $\Gamma = \Gamma_{\text{S}} + \Gamma_{\text{D}}$. The dimensionless quantity $\xi = \pi^2 v_{\text{S}} v_{\text{D}} W^2$ defines the direct tunneling coupling between two leads, and $v_{\text{S/D}}$ stands for the density of states of the source or the drain lead, respectively. $\text{Re}G_d^r(\omega)$ and $\text{Im}G_d^r(\omega)$ are the real and imaginary parts of the dot retarded Green function defined as

$$G_d^r(\omega) = -i \int dt e^{i\omega t} \theta(t) \langle \{d_1, e^{iHt} d_1^\dagger e^{-iHt}\} \rangle. \quad (\text{B5})$$

Employing the same treatment as to the double-dot interferometer, we finally obtain the imaginary part of the dot retarded Green function in the presence of EPI as

$$\begin{aligned} \text{Im}G_d^r(\omega) &= -\frac{i}{2} [G_d^>(\omega) - G_d^<(\omega)] \\ &= -\frac{i}{2} \sum_n L_n [\overline{G}_d^>(\omega - n\omega_0) - \overline{G}_d^<(\omega + n\omega_0)], \end{aligned} \quad (\text{B6})$$

where the decoupled lesser and greater Green functions are

$$\begin{aligned} \overline{G}_d^<(\omega) &= \frac{i|\overline{G}_d^r(\omega)|^2}{(1 + \xi)^2} \left[2 \sqrt{\xi \Gamma_{\text{S}} \Gamma_{\text{D}}} \sin \phi (f_{\text{S}} - f_{\text{D}}) \right. \\ &\quad \left. + (\bar{\Gamma}_{\text{S}} + \xi \bar{\Gamma}_{\text{D}}) f_{\text{S}} + (\bar{\Gamma}_{\text{D}} + \xi \bar{\Gamma}_{\text{S}}) f_{\text{D}} \right], \end{aligned} \quad (\text{B7})$$

and

$$\begin{aligned} \overline{G}_d^>(\omega) &= -\frac{i|\overline{G}_d^r(\omega)|^2}{(1 + \xi)^2} \left[-2 \sqrt{\xi \Gamma_{\text{S}} \Gamma_{\text{D}}} \sin \phi (f_{\text{S}} - f_{\text{D}}) \right. \\ &\quad \left. + (\bar{\Gamma}_{\text{S}} + \xi \bar{\Gamma}_{\text{D}})(1 - f_{\text{S}})(\bar{\Gamma}_{\text{D}} + \xi \bar{\Gamma}_{\text{S}})(1 - f_{\text{D}}) \right]. \end{aligned} \quad (\text{B8})$$

Here the module square of the decoupled retarded Green function is

$$|\overline{G}_d^r(\omega)|^2 = \left\{ [\omega - (\epsilon_0 - \frac{\lambda^2}{\omega_0}) + \frac{\sqrt{\xi \Gamma_{\text{S}} \Gamma_{\text{D}}}}{1 + \xi} \cos \phi]^2 + (\frac{1}{2} \frac{\bar{\Gamma}_{\text{S}} + \bar{\Gamma}_{\text{D}}}{1 + \xi})^2 \right\}^{-1},$$

and the renormalized dot-lead coupling reads

$$\bar{\Gamma}_{\text{S(D)}} = \Gamma_{\text{S(D)}} \exp[-2(\lambda/\omega_0)^2 (N_{\text{ph}} + 1/2)]. \quad (\text{B9})$$

Then, by the Kramers-Kronig relation

$$\text{Re}G_d^r(\omega) = - \int \frac{d\omega'}{\pi} \text{Re}[\frac{\text{Im}G_d^r(\omega')}{\omega - \omega' + i0^+}]. \quad (\text{B10})$$

The real part of the retarded Green function in Eq. (B4) can be easily obtained.

* Electronic address: luhaizhou@gmail.com

† Electronic address: bfz@tsinghua.edu.cn

¹ L. L. Sohn, L. P. Kouwenhoven, and G. Schön, eds., *Mesoscopic Electron Transport, NATO Advanced Study Institutes, Ser. E*, vol. 345 (Kluwer, Dordrecht, 1997).

² A. Yacoby, Phys. Rev. Lett. **74**, 4047 (1995).

³ R. Schuster, E. Buks, M. Heiblum, D. Mahalu, V. Umansky, and H. Shtrikman, Nature (London) **385**, 417 (1997).

⁴ K. Kobayashi, H. Aikawa, S. Katsumoto, and Y. Iye, Phys. Rev. Lett. **88**, 256806 (2002).

⁵ H. Aikawa, K. Kobayashi, A. Sano, S. Katsumoto, and Y. Iye, Phys. Rev. Lett. **92**, 176802 (2004).

⁶ E. Buks, R. Schuster, M. Heiblum, D. Mahalu, and V. Umansky, Nature(London) **391**, 871 (1998).

⁷ A. P. Jauho and N. S. Wingreen, Phys. Rev. B **58**, 9619 (1998).

⁸ J. Park, A. Pasupathy, J. Goldsmith, C. Chang, Y. Yaish, J. Petta, M. Rinkoski, J. Sethna, H. Abruna, and P. McEuen, Nature (London) **417**, 722 (2002).

⁹ L. H. Yu, Z. K. Keane, J. W. Ciszek, L. Cheng, M. P. Stewart, J. M. Tour, and D. Natelson, Phys. Rev. Lett. **93**, 266802 (2004).

¹⁰ B. J. LeRoy, S. G. Lemay, J. Kong, and C. Dekker, Nature (London) **432**, 371 (2004).

¹¹ B. Kubala and J. König, Phys. Rev. B **65**, 245301 (2002).

¹² F. Marquardt and C. Bruder, Phys. Rev. B **68**, 195305 (2003).

¹³ M. A. Reed, C. Zhou, C. J. Muller, T. P. Burgin, and J. M. Tour, Science **278**, 252 (1997).

¹⁴ A. Nitzan and M. A. Ratner, Science **300**, 1384 (2000).

¹⁵ B. C. Stipe, M. A. Rezaei, and W. Ho, Science **280**, 1732 (1998).

¹⁶ H. Park, J. Park, A. K. L. Lim, E. H. Anderson, A. P. Alivisatos, and P. L. McEuen, Nature (London) **407**, 57 (2000).

¹⁷ N. B. Zhitenev, H. Meng, and Z. Bao, Phys. Rev. Lett. **88**, 226801 (2002).

¹⁸ A. N. Pasupathy, J. Park, C. Chang, A. V. Soldatov, S. Lebedkin, R. C. Bialczak, J. E. Grose, L. A. K. Donev, J. P. Sethna, D. C. Ralph, et al., Nano lett. **5**, 203 (2005).

¹⁹ S. Sapmaz, P. Jarillo-Herrero, Y. Blanter, C. Dekker, and H. S. J. van der Zant, Phys. Rev. Lett. **96**, 026801 (2006).

²⁰ O. Entin-Wohlman, Y. Imry, and A. Aharony, Phys. Rev. B **70**, 075301 (2004).

²¹ A. Ueda and M. Eto, Phys. Rev. B **73**, 235353 (2006).

²² Z. Ma, Y. Zhu, X.-Q. Li, T.-H. Lin, and Z.-B. Su, Phys. Rev. B **69**, 045302 (2004).

²³ A. P. Jauho and P. Minnhagen, J. Phys. C: Solid State Phys. **17**, 4369 (1984).

²⁴ J. W. A. III, W. Walukiewicz, M. McCluskey, M. A. Plano, and M. I. Landstrassb, Appl. Phys. Lett. **66**, 616 (1994).

²⁵ A. P. Jauho, N. S. Wingreen, and Y. Meir, Phys. Rev. B **50**, 5528 (1994).

²⁶ M. L. de Guevara, F. Claro, and P. A. Orellana, Phys. Rev. B **67**, 195335 (2003).

²⁷ H. Lu, R. Lü, and B.-F. Zhu, Phys. Rev. B **71**, 235320 (2005).

²⁸ G. D. Mahan, *Many-Particle Physics* (Plenum Press, New York, 1990).

²⁹ H. Lu, Z.-Z. Chen, R. Lü, and B.-F. Zhu, Phys. Stat. Sol. (c) **4**, 574 (2006).

³⁰ Z.-Z. Chen, R. Lu, and B.-F. Zhu, Phys. Rev. B **71**, 165324 (2005).

³¹ J. Friedel, Adv. Phys. **3**, 446 (1953).

³² W. Hofstetter, J. König, and H. Schoeller, Phys. Rev. Lett. **87**, 156803 (2001).